Flux-Coordinate Splitting Technique for the Navier-Stokes Equations

R. M. C. So* and H. S. Zhang†
Arizona State University, Tempe, Arizona 85287

The method of fractional steps is used to split the unsteady, two-dimensional Navier-Stokes equations into a set of Euler equations and a diffusion-type equation. A flux-coordinate splitting technique is used to solve the Euler equations so that shocks and contact discontinuities are resolved sharply in gasdynamic flows. The technique involves solving the Euler equations everywhere in the flowfield using a flux-vector splitting technique except in small regions surrounding the contact discontinuities. In these regions, the method of fractional steps is again used to split the Euler equations into a set of one-dimensional equations. These equations are then transformed into Lagrangian form with no explicit density dependence in the spatial derivatives. Since the total velocity and pressure are continuous across a contact discontinuity, the boundary conditions of the transformed Lagrangian equations are automatically connected. Solutions of these equations, therefore, give a very sharp contact discontinuity. All the equations—the one-dimensional Lagrangian, the two-dimensional Eulerian, and the diffusion-type equations—are solved using a second-order accurate finite-difference scheme. Validations of the technique are carried out with exact solutions of the flow in a shock tube and the mixing of two supersonic streams at different initial pressures and densities. Good agreement is obtained, especially the infinite resolution of the contact discontinuity. Furthermore, viscous effects do not seem to have a significant influence on the resolution of the contact discontinuity.

I. Introduction

MANY practical internal flow problems involve shocks, contact discontinuities, and/or material interfaces. A few of these examples are the flows in pressure-wave superchargers, centrifugal compressors, and screw pumps where the fluid changes phase. The simultaneous presence of shocks, contact discontinuities, and/or material interfaces renders the flowfields very complicated to calculate. For example, flux-vector splitting techniques developed for one- and two-dimensional external flows[1-4] can be applied to solve the conservation-law form of the governing equations and allow shocks in the flow to be captured as weak solutions to the equations. Consequently, the difficulty of applying shock-fitting techniques[5,6] to arbitrary flows can be avoided, and an accurate shock capturing technique is now available for two-dimensional flows with shocks.[3,4] These techniques have also been successfully applied to internal flows.[7-10] However, their applications to three-dimensional internal flows with shocks and contact discontinuities remain a difficult task.

Even though the flux-vector splitting techniques can capture shocks and contact discontinuities and are able to resolve correctly the locations and strength of the shocks, they fail to correctly resolve contact discontinuities. The reason is that the techniques lead to numerical diffusion and/or dispersion of a contact discontinuity and hence numerical smearing. Techniques where both shocks and contact discontinuities in one-dimensional flows are resolved sharply have been proposed by various researchers.[11-15] Among the more notable examples are the artificial compression method (ACM),[11] the essentially nonoscillatory scheme (ENO),[12] the ENO/subcell and ENO/ACM methods,[13] and the random choice technique.[14,15] All these techniques are able to reduce numerical smearing to a minimum when used to solve gasdynamic equations. With the exception of the random choice technique, which gives infinite resolution to the calculated shocks and contact discontinuities, the best resolution offered by other numerical methods, such as ENO/subcell and ENO/ACM,[13] is about three grid cells for both shocks and contact discontinuities. In spite of its ability to give infinite resolution for shocks and contact discontinuities, the random choice technique has one drawback. Due to the random nature of the technique, the calculated positions of the shocks and contact discontinuities are only correct in an averaged sense.[16,17] In addition, the calculated rarefaction is not smooth because of the technique's inherent randomness.[17] This drawback could have a significant effect on the calculation of two-dimensional internal gasdynamic flows where viscous wall boundary conditions are required to be satisfied by the governing equations, and the interactions of shocks and contact discontinuities with wall boundary layers could result. As for other techniques,[11,12] the improved resolution is often achieved through the use of higher-order accurate numerical schemes. Therefore, there is a need for a simple technique that can resolve shocks and contact discontinuities sharply and yet does not require a numerical scheme that is third- or higher-order accurate. Furthermore, it should be fairly easy to apply to external as well as internal flow problems, such as those encountered in a pressure-wave supercharger.[18]

Recently, a flux-coordinate splitting technique has been proposed for the capturing of shocks and contact discontinuities in steady and unsteady one- and two-dimensional gasdynamic flows.[19] The technique employs flux-vector splitting[1-4] to solve the governing Euler equations over most of the flowfield, except in small regions surrounding the contact discontinuities. Therefore, shocks in the flow can be captured with precision. The method of fractional steps[20-22] is applied to split the Euler equations in the regions surrounding the contact discontinuities. As a result, the split equations are one-dimensional and the transformation of Richtmyer and Morton[23] is generalized to transform the set of split equations to Lagrangian form. In the transformed equations, density does not appear explicitly in the spatial derivatives. Therefore, the dependent variables are continuous across the discontinuities and could be solved using any finite-difference scheme without introducing numerical smearing to the calculation of the discontinuities. The contact discontinuities thus resolved are very sharp indeed. Validations of the technique[19] have been carried out with a

Received July 17, 1989; revision received April 17, 1990; accepted for publication Aug. 21, 1990.

*Professor, Mechanical and Aerospace Enginering.
†Graduate Assistant, Mechanical and Aerospace Engineering.

one-dimensional shock tube flow, a converging cylindrical shock flow and a steady, two-dimensional supersonic mixing flow. In each of these cases, the contact discontinuity has been calculated with infinite resolution, whereas the shock and expansion waves are resolved accurately compared with other shock capturing schemes. These results are accomplished using a conventional second-order accurate finite-difference scheme. Therefore, a simple yet accurate shock and contact discontinuity capturing scheme is now available for extension to viscous gasdynamic flows.

The objective of the present paper is to extend the flux-coordinate splitting technique[19] to solve the Navier-Stokes equations. Various procedures to handle the viscous terms in a finite-difference solution of the compressible Navier-Stokes equations have been proposed.[24,25] Since the flux-coordinate splitting technique relies on splitting the Euler equations in both time and spatial coordinates, it is rather tedious numerically to keep track of the viscous contributions in each of the split equations. An alternative would be to use the recently proposed split scheme for Navier-Stokes equations.[26] However, for the present application, a logical approach to solve the Navier-Stokes equations would be to apply the method of fractional steps[20-22] to first split the Navier-Stokes equations into a set of Euler equations and a diffusion-type equation. The flux-coordinate splitting technique could then be used to solve the Euler equations, whereas the diffusion-type equation could be solved using a finite difference scheme of comparable accuracy. This way, the viscous terms in the Navier-Stokes equations could be treated in a formal way without introducing unnecessary complication in the numerical scheme and the flux-coordinate splitting technique could again be used to capture shocks and contact discontinuities accurately in a viscous flow. The procedure has already been applied to calculate practical flows with axial symmetry[18] and could be extended to three-dimensional flows.

II. Governing Equations

Unsteady, two-dimensional, laminar compressible flow of a Newtonian fluid is considered. The Navier-Stokes equations with velocity vector $W=(W_x, W_y)$ in Cartesian coordinates (x,y) can be concisely written as

$$\frac{\partial U}{\partial t}+\frac{\partial F(U)}{\partial x}+\frac{\partial G(U)}{\partial y}+\frac{\partial H_x}{\partial x}+\frac{\partial H_y}{\partial y}=0 \tag{1}$$

where

$$U=\begin{bmatrix}\rho\\ \rho W_x\\ \rho W_y\\ e\end{bmatrix} \tag{2a}$$

$$F=\begin{bmatrix}\rho W_x\\ \rho W_x^2+p\\ \rho W_x W_y\\ (e+p)W_x\end{bmatrix} \tag{2b}$$

$$G=\begin{bmatrix}\rho W_y\\ \rho W_x W_y\\ \rho W_y^2+p\\ (e+p)W_y\end{bmatrix} \tag{2c}$$

$$H_x=\begin{bmatrix}0\\ -\tau_{xx}\\ -\tau_{xy}\\ -k\dfrac{\partial T}{\partial y}-\tau_{xy}W_x-\tau_{yy}W_y\end{bmatrix} \tag{2d}$$

$$H_y=\begin{bmatrix}0\\ -\tau_{xy}\\ -\tau_{yy}\\ -k\dfrac{\partial T}{\partial y}-\tau_{xy}W_x-\tau_{yy}W_y\end{bmatrix} \tag{2e}$$

$$\tau_{xx}=\mu\left[2\frac{\partial W_x}{\partial x}-\frac{2}{3}\nabla\cdot W\right] \tag{2f}$$

$$\tau_{yy}=\mu\left[2\frac{\partial W_y}{\partial y}-\frac{2}{3}\nabla\cdot W\right] \tag{2g}$$

$$\tau_{xy}=\mu\left[\frac{\partial W_x}{\partial y}-\frac{\partial W_y}{\partial x}\right] \tag{2h}$$

$$\nabla\cdot W=\frac{\partial W_x}{\partial x}+\frac{\partial W_y}{\partial y} \tag{2i}$$

The perfect gas equation is given by

$$p=(\gamma-1)\left[e-\tfrac{1}{2}\rho(W_x^2+W_y^2)\right] \tag{3}$$

In these equations, p, ρ, and T are pressure, density, and temperature, respectively, e is the total energy per unit volume, γ is the specific heat ratio, μ is fluid viscosity, and k is thermal conductivity. The fluid properties μ and k are assumed to be temperature dependent. Their evaluations are explained in Sec. IV when the sample calculations are discussed.

The basic idea of the method of fractional steps[20] is to apply a time splitting to Eq. (1). This way, the Navier-Stokes equations are split into a set of Euler equations and a diffusion-

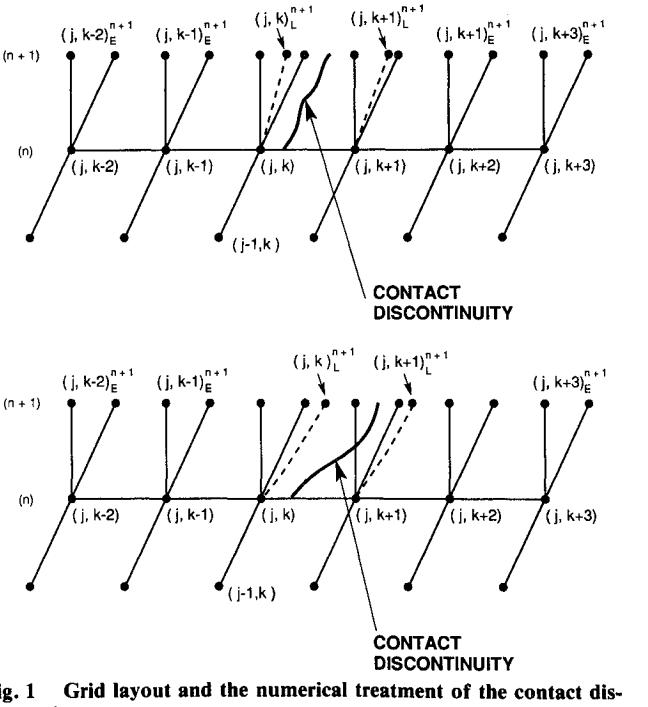

Fig. 1 Grid layout and the numerical treatment of the contact discontinuity.

type equation that includes all the viscous terms. Following this procedure, the split equations can be written as

$$\frac{\partial (U)_f}{\partial t} + \frac{\partial F}{\partial x} + \frac{\partial G}{\partial y} = 0 \tag{4}$$

$$\frac{\partial U}{\partial t} + \frac{\partial H_x}{\partial x} + \frac{\partial H_y}{\partial y} = 0 \tag{5}$$

where F, G, H_x, and H_y are functions of $(U)_f$, which represents the solution of the Euler equations. However, $(U)_f$ is not the solution of Eq. (1). The solution of Eq. (1) is given by the solutions of Eqs. (4) and (5), where H_x and H_y are evaluated based on $(U)_f$. Therefore, Eq. (4) can be solved using either the flux-coordinate splitting technique[19] or other equally accurate numerical schemes,[13,27] and Eq. (5) can be solved by conventional finite-difference schemes.

III. Flux-Coordinate Splitting Technique

The basic idea of flux-coordinate splitting is to use flux-vector splitting to capture shocks and contact discontinuities and to use a Lagrangian technique to sharpen the captured contact discontinuities in the flowfield. Therefore, in the following, the flux-vector splitting technique is briefly described first. This is followed by a discussion of the coordinate splitting technique, the numerical algorithms used, and the numerical procedure proposed for sharpening the contact discontinuity. Since the stability and accuracy of the flux-coordinate splitting technique has been analyzed, the interested reader is referred to Ref. 19 for details.

Flux-Vector Splitting

Different flux-vector splitting schemes have been proposed.[1-4] Basically, the technique involves splitting the flux vector into a forward and a backward contribution and is usually accomplished by splitting the eigenvalues of the Jacobian matrix of the full flux into negative and positive groups. However, not all schemes produce continuously differentiable split fluxes. One exception is the scheme proposed by van Leer,[2] which has since been generalized to two-dimensional flows by Anderson et al.[4] The present approach adopts the scheme proposed by van Leer.[2] Details of this scheme can be found in Refs. 2 and 4.

Coordinate Splitting

The method of fractional steps[20] is used to split Eq. (4) into a set of one-dimensional equations

$$\frac{1}{2}\frac{\partial (U)_f}{\partial t} + \frac{\partial F}{\partial x} = 0 \tag{6}$$

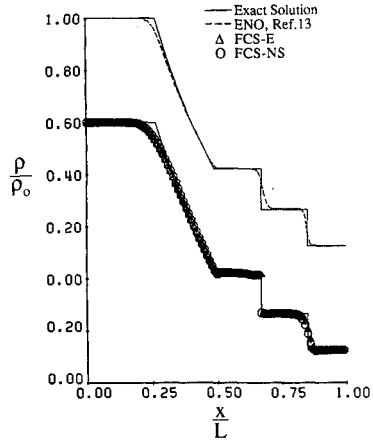

Fig. 2 Density distribution in a shock tube flow for the high pressure ratio case.

$$\frac{1}{2}\frac{\partial (U)_f}{\partial t} + \frac{\partial G}{\partial y} = 0 \tag{7}$$

where F and G are functions of $(U)_f$. These equations still have density appearing explicitly in F and G. Therefore, a straightforward finite-difference solution of these equations will lead to smearing of the contact discontinuities.[2] Zhang and So[19] proposed to generalize the Richtmyer and Morton[23] transformation to transform Eqs. (6) and (7) to Lagrangian form with no explicit density dependence in the spatial derivatives. The generalized transformation can be written as

$$\frac{1}{2}\left(\frac{\partial}{\partial t}\right)_L = \left[\frac{1}{2}\frac{\partial}{\partial t} + W_x\frac{\partial}{\partial x}\right]_E \tag{8a}$$

$$\left(\frac{\partial \xi}{\partial x}\right)_y = \rho \tag{8b}$$

for the x direction and

$$\frac{1}{2}\left(\frac{\partial}{\partial t}\right)_L = \left[\frac{1}{2}\frac{\partial}{\partial t} + W_y\frac{\partial}{\partial y}\right]_E \tag{9a}$$

$$\left(\frac{\partial \eta}{\partial y}\right)_x = \rho \tag{9b}$$

for the y direction, where the subscripts E and L are used to denote the Eulerian and Lagrangian frame of reference, respectively. In the transformation Eq. (8b), y is kept constant, whereas x is kept constant in Eq. (9b). After applying the transformations Eqs. (8) and (9) to Eqs. (6) and (7), the following is obtained:

$$\frac{1}{2}\frac{\partial V}{\partial t} + \frac{\partial A(V)}{\partial \xi} = 0 \tag{10}$$

$$\frac{1}{2}\frac{\partial V}{\partial t} + \frac{\partial B(V)}{\partial \eta} = 0 \tag{11}$$

where

$$V = \begin{bmatrix} \rho^{-1} \\ W_x \\ W_y \\ e\rho^{-1} \end{bmatrix} \tag{12a}$$

$$A = \begin{bmatrix} W_x \\ p \\ 0 \\ pW_x \end{bmatrix} \tag{12b}$$

$$B = \begin{bmatrix} W_y \\ p \\ 0 \\ pW_y \end{bmatrix} \tag{12c}$$

The subscript L has been dropped from $(\partial/\partial t)$ and, as expected, ρ does not appear explicitly in A and B. This together with the fact that p and $|W|$ are continuous across a contact discontinuity allows the discontinuity to be resolved sharply even when Eqs. (10) and (11) are solved using finite-difference methods.

Numerical Algorithms

Zhang and So[19] use the alternating explicit upwind and MacCormack scheme[27] to solve the split flux equations. The

scheme is second-order accurate and gives rise to a 3–4 grid cell resolution of the shock. In addition, they use the MacCormack scheme[22] to solve the transformed Lagrangian equations and show that the overall accuracy of the combined solution is second order and that the numerical solution is fairly stable. The contact discontinuity has been calculated with infinite resolution, and there is no need to use higher-order numerical schemes to improve the accuracy of the solution. Of course, a third- or fourth-order accurate scheme could be used to solve the split flux equations. To be consistent, an equivalent scheme has to be used to solve the transformed Lagrangian equations. Since this cannot improve the resolution of the contact discontinuity any further, a more complicated numerical scheme is not necessary. Consequently, there is no need to employ a numerical scheme that is more than second-order accurate to solve the governing equations.

In view of the preceding discussion, the numerical schemes of Ref. 19 are applied to solve Eqs. (4), (5), (10), and (11) using a fixed grid shown in Fig. 1. In Fig. 1, the index j is used to denote increments along the x axis so that $x = j\Delta x$. Similarly, the indices k and n denote increments along the y axis and the time coordinate so that $y = k\Delta y$ and $t = n\Delta t$. The figure shows the grid points at two time steps, those of n and $(n+1)$. Figure 1a shows the situation where the contact discontinuity moves within the same grid cell in one time step, and Fig. 1b illustrates the case where the contact discontinuity moves to a different grid cell in one time step. The numerical procedure used to handle these two different situations is explained in the following section. For odd values of n, the explicit upwind scheme is used to solve Eq. (4) and the finite-difference equations are

$$\overline{U_{j,k}^{n+1}} = U_{j,k}^{n} - \frac{\Delta t}{\Delta x}\left[\Delta_x(F_{j,k}^{-})^n + \nabla_x(F_{j,k}^{+})^n\right] - \frac{\Delta t}{\Delta x}\left[\Delta_y(G_{j,k}^{-})^n + \nabla_y(G_{j,k}^{+})^n\right] \tag{13a}$$

$$U_{j,k}^{n+1} = \frac{1}{2}\left(U_{j,k}^{n} + \overline{U_{j,k}^{n+1}}\right) - \frac{\Delta t}{2\Delta x}\left[\Delta_x(F_{j,k}^{-})^{\overline{n+1}} + \nabla_x(F_{j,k}^{+})^{\overline{n+1}}\right] - \frac{\Delta t}{2\Delta y}\left[\Delta_y(G_{j,k}^{-})^{\overline{n+1}} + \nabla_y(G_{j,k}^{+})^{\overline{n+1}}\right] - \frac{\Delta t}{2\Delta x}\left[\nabla_x^2(F_{j,k}^{+})^n + \Delta_x^2(F_{j,k}^{-})^n\right] - \frac{\Delta t}{2\Delta y}\left[\nabla_y^2(G_{j,k}^{+})^n + \Delta_y^2(G_{j,k}^{-})^n\right] \tag{13b}$$

whereas for even values of n, the MacCormack scheme is used to advance the solution. The finite-difference equations for this scheme are the same as Eq. (13) with terms involving Δ^2 and ∇^2 set equal to zero. Here, $U_{j,k}^{n+1}$ is the predictor value, whereas $U_{j,k}^{n+1}$ is the corrector value, $F^{\pm}$ and $G^{\pm}$ are the split fluxes of F and G, respectively, and the forward and backward difference operators are defined as

$$\Delta_x(F_{j,k}^{n}) = F_{j+1,k}^{n} - F_{j,k}^{n} \tag{14a}$$

$$\Delta_y(G_{j,k}^{n}) = G_{j,k+1}^{n} - G_{j,k}^{n} \tag{14b}$$

$$\nabla_x(F_{j,k}^{n}) = F_{j,k}^{n} - F_{j-1,k}^{n} \tag{14c}$$

$$\nabla_y(G_{j,k}^{n}) = G_{j,k}^{n} - G_{j,k-1}^{n} \tag{14d}$$

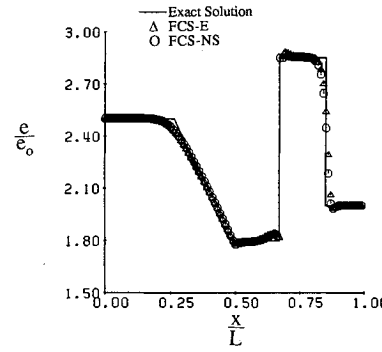

Fig. 3 Energy distribution in a shock tube flow for the high pressure ratio case.

Once Eq. (4) is solved, Eq. (5) is obtained from the finite-difference equation,

$$\hat{U}_{j,k}^{n+1} = U_{j,k}^{n+1} - \Delta t\left[\frac{\partial H_x}{\partial x} + \frac{\partial H_y}{\partial y}\right]_{j,k} \tag{15}$$

where $U_{j,k}^{n+1} = [U(j\Delta x, k\Delta y)]_f$ is the solution of Eq. (4). In discretizing the square bracketed term in Eq. (15), a central difference scheme suggested by MacCormack[25] is used. The resultant finite-difference equations are too cumbersome, therefore, they are not given here. Equations (10) and (11) are solved by the MacCormack scheme[22] and the finite-difference equations are

$$\overline{V_{j,k}^{n+1/2}} = V_{j,k}^{n} - \frac{\Delta t}{\Delta \eta}\nabla_\eta(B_{j,k}^{n}) \tag{16a}$$

$$V_{j,k}^{n+1/2} = \frac{1}{2}\left(V_{j,k}^{n} + \overline{V_{j,k}^{n+1/2}}\right) - \frac{\Delta t}{2\Delta \eta}\Delta_\eta(\overline{B_{j,k}^{n+1/2}}) \tag{16b}$$

$$\overline{V_{j,k}^{n+1}} = \overline{V_{j,k}^{n+1/2}} - \frac{\Delta t}{\Delta \xi}\nabla_\xi(A_{j,k}^{n+1/2}) \tag{16c}$$

$$V_{j,k}^{n+1} = \frac{1}{2}\left(V_{j,k}^{n+1/2} + \overline{V_{j,k}^{n+1}}\right) - \frac{\Delta t}{2\Delta \xi}\Delta_\xi(\overline{A_{j,k}^{n+1}}) \tag{16d}$$

The detailed procedure of solving Eqs. (13), (15), and (16) is discussed next.

Sharpening of the Contact Discontinuity

The flux-coordinate splitting technique is used to sharpen the contact discontinuity once it has been captured by the flux-vector splitting technique, which is accomplished by solving Eq. (13). If the present technique is used to solve steady flow problems, Eq. (13) is solved until the solutions at two consecutive time steps are essentially identical. When the flux-vector splitting solution is available, the location of the contact discontinuity is determined as follows. The location of the midpoint of the spread of the contact discontinuity is obtained from the flux-vector splitting solution. It is taken to be the approximate location of the contact discontinuity. The flux-vector splitting solution is assumed to be the initial state of the transformed Lagrangian equations, and Eq. (16) is used to forward march to the next time step. The location of the contact discontinuity at the new time step is given by

$$x^{n+1} = x^{n} + W_x^{n}\Delta t \tag{17a}$$

$$y^{n+1} = y^{n} + W_y^{n}\Delta t \tag{17b}$$

where $(\,)^n$ is used to denote the property at time step $n\Delta t$, and x^n and y^n are known from the flux-vector splitting solution. The Lagrangian grid points and their associated properties thus determined are used to calculate the Eulerian properties at the grid points surrounding the discontinuity. Here, two situa-

tions can arise. The discontinuity can move within the same grid cell (Fig. 1a), or it can move to another grid cell (Fig. 1b) in one time step.

In the first case (Fig. 1a), the properties at $(j,k)_E^{n+1}$ and $(j,k+1)_E^{n+1}$ are not known, where subscript E denotes the Eulerian point. However, the properties at all other Eulerian grid points are known from solving Eq. (13), and the properties at $(j,k)_L^{n+1}$ and $(j,k+1)_L^{n+1}$ are known from solving Eq. (16). Here, the subscript L is used to denote the Lagrangian point. This means that the properties at the points $(j,k-2)_E^{n+1}$, $(j,k-1)_E^{n+1}$, and $(j,k)_L^{n+1}$ can be used to interpolate the properties at $(j,k)_E^{n+1}$. Similarly, the points $(j,k+3)_E^{n+1}$, $(j,k+2)_E^{n+1}$, and $(j,k+1)_L^{n+1}$ are used to extrapolate the properties at $(j,k+1)_E^{n+1}$. The location of the discontinuity at the new time step is then corrected by solving

$$x^{n+1} = x^n + \tfrac{1}{2}(W_x^{n+1} + W_x^n)\Delta t \tag{18a}$$

$$y^{n+1} = y^n + \tfrac{1}{2}(W_y^{n+1} + W_y^n)\Delta t \tag{18b}$$

before advancing to the next time step.

In the second case (Fig. 1b), $(j,k+1)_E^{n+1}$ and $(j,k)_E^{n+1}$ are on the same side of the discontinuity. If an extrapolation formula is used to determine the properties at $(j,k+1)_E^{n+1}$, smearing of the discontinuity would result because the points $(j,k+3)_E^{n+1}$, $(j,k+2)_E^{n+1}$, and $(j,k)_E^{n+1}$ are on the opposite side of the discontinuity from $(j,k+1)_E^{n+1}$. Since p and $|W|$ are continuous across a contact discontinuity, extrapolation formulas can again be used to determine these properties at $(j,k+1)_E^{n+1}$. As for density at $(j,k+1)_E^{n+1}$, the approximation is made that it is equal to the density at $(j,k)_L^{n+1}$. The energy e at $(j,k+1)_E^{n+1}$ is then determined from Eq. (3). Since the points $(j,k-2)_E^{n+1}$, $(j,k-1)_E^{n+1}$, $(j,k)_L^{n+1}$ are all on the same side of the discontinuity, interpolation formulas can be used to determine all properties at $(j,k)_E^{n+1}$. The solution is forward marched in time until steady-state condition is reached. At this point, Eq. (15) is solved to give the final solution to the problem.

The procedure described earlier for steady flow can also be used to calculate unsteady flow problems. In this case, the flux-vector splitting technique is first used to advance the solution to $t = m\Delta t$. Then the flux-coordinate splitting technique is used to advance the solution to $t = n\Delta t$ where $n > m$. This way, the error incurred by Eqs. (16) and (18) in the determination of the discontinuity location could be reduced to a minimum, and the discontinuity could still be sharpened substantially. It should be pointed out that Eq. (15) is solved at every time step following the application of the flux-coordinate splitting technique.

Finally, the question of shock crossing should be addressed. This is discussed in detail in Ref. 19. Therefore, it only needs to be pointed out here that when a shock crosses a contact discontinuity, the flux-coordinate splitting technique is suppressed for a few time steps to allow the flux-vector splitting technique to handle the crossing problem. The effect of this suppression on the overall calculation is negligible as demonstrated by the analysis of Ref. 19. There are other methods to deal with this problem; however, addressing the question this way greatly simplifies the numerical complexities involved in the calculation of the crossing between a shock and a contact discontinuity.

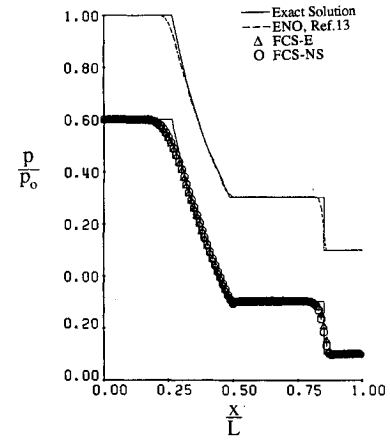

Fig. 4 Pressure distribution in a shock tube flow for the high pressure ratio case.

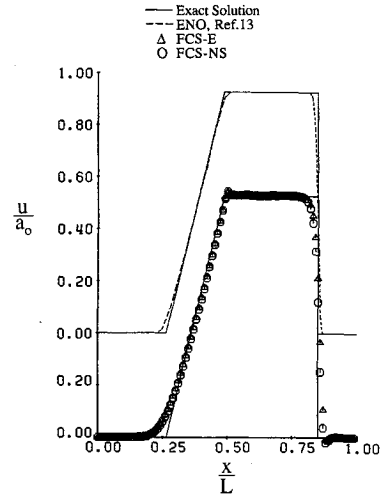

Fig. 5 Mach number distribution in a shock tube flow for the high pressure ratio case.

IV. Results and Discussion

Two sample gasdynamic flow problems involving shocks and contact discontinuities and with known exact Euler solutions are chosen for validation of the present technique. One is the gasdynamic flow in a shock tube. This is an unsteady, one-dimensional problem; the exact solution of which is available in any standard text, such as Ref. 28. In addition to the exact solution, the problem has also been calculated by various researchers in an effort to verify their techniques. Consequently, comparisons with other numerical calculations such as ENO,[13] ENO/ACM,[13] and ENO/subcell[13] are also carried out. Another is a steady, two-dimensional mixing of two supersonic streams. An exact solution of this problem can be found in Ref. 29. The problem has also been solved using different numerical techniques.[30,31] Consequently, the present solution can be compared with all these results, and the relative merits of the proposed technique can be evaluated. Together, these two sample problems allow the present technique to be evaluated for its accuracy in the resolution of shocks and contact discontinuities for steady and unsteady, one-and two-dimensional viscous gasdynamic flows. Therefore, this paves the way for the application of the technique to calculate internal gasdynamic flows where viscous effects are important near a wall[18]

All calculations are carried out in a VAX 8650 computer. For the shock tube problem, the calculations only take a few seconds of CPU time to complete. On the other hand, the two-dimensional problem requires about 6000 s of CPU time. It takes 820 iterations to obtain a convergent solution to Eq. (4) using the flux-vector splitting technique alone. Sharpening the contact discontinuity using the flux-coordinate splitting technique requires about 30 more iterations. Therefore, the flux-coordinate splitting technique does not put a heavy burden on the overall CPU time.

Shock Tube Flow

The governing equations for this problem are the same as the two-dimensional equations but with $W_y = 0$ and $\partial(\ )/\partial y \equiv 0$. In this case, coordinate splitting is not necessary be-

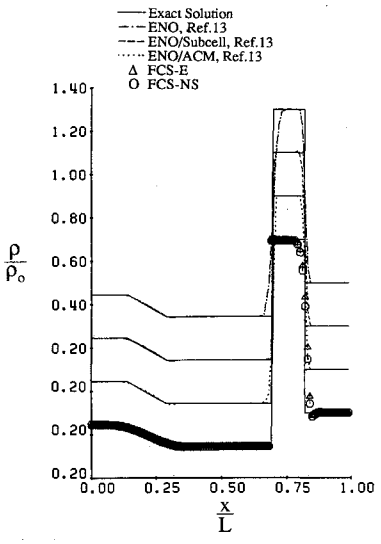

Fig. 6 Density distribution in a shock tube flow for the low pressure ratio case.

cause the Richtmyer and Morton transformation can be applied directly to Eq. (4) to transform it to Eq. (10). These equations are used to solve an idealized shock tube problem. The diaphragm used to separate the high pressure gas from the low pressure gas is located at $x/L = 0.5$, where L is the length of the shock tube. At time $t = 0$, the diaphragm ruptures, sending a shock followed by a contact discontinuity into the low-pressure chamber, and an expansion wave into the high-pressure chamber. The calculation are carried out assuming perfect gas ($\gamma = 1.4$) for initial conditions of $(\rho, W_x, p)_L = (1,0,1)$ and $(\rho,\ W_x,\ p)_R = (0.125,\ 0,\ 0.10)$ in the high- and low-pressure regions, respectively, with a $\Delta x/L = 0.01$ and a time step of $\Delta t = \mathrm{CFL}(\Delta x)/\max(|W_x| + a)$. Here, CFL is a constant, subscript L denotes the left side of the diaphragm and R the right side. A CFL = 0.3 is chosen for all calculations. To compare with the ENO results, a second calculation with initial conditions of $(\rho,\ W_z,\ p)_L = (0.445,\ 0.698,\ 3.528)$ and $(\rho, W_x, p)_R = (0.5,0,\ 0.571)$, respectively, is also carried out. In carrying out these calculations, the fluid properties μ and k are evaluated in the following manner. Mean μ and k are defined so that $2\bar{\mu} = \mu_L + \mu_R$ and $2\bar{k} = k_L + k_R$, whereas the μ_L, μ_R, k_L, and k_R are calculated based on the temperatures on either side of the shock or contact discontinuity. Once the mean μ and k are determined, they are assumed constant in the governing equations. The results are presented in terms of ρ/ρ_o, e/e_o, p/p_o, and W_x/a_o vs x/L at a fixed t, where a_o, p_o, and ρ_o are the sound speed, pressure, and density of the stationary high-pressure gas and $e_o = p_o/[\rho_o(\gamma - 1)]$.

Figures 2-5 show the results of the case where the initial pressure ratio is high. As for the case where the initial pressure ratio is low, only the ρ/ρ_o result is given in Fig. 6. Up to six different results are shown in these figures for comparisons. In addition to the exact solutions, the present calculations using Euler and Navier-Stokes equations are shown. The abbreviations FCS-E and FCS-NS are used to denote the flux-coordinate splitting solutions of the Euler and Navier-Stokes equations, respectively. Besides these solutions, the ENO, ENO/ACM, and ENO/subcell results extracted from Ref. 13 are also shown in Figs. 2-6. To minimize clutter, the ENO, ENO/ACM, and ENO/subcell results are plotted in the same figure but with the origin shifted by one or two divisions. Furthermore, in each plot the exact solution is shown to facilitate comparison of the accuracy of each method.

It can be seen that the contact discontinuity is again calculated with infinite resolution (Figs. 2, 3, and 6); that is, the number of grid cells over which the density variation occurs in zero. This could be explained as follows. The present calculations solve Eq. (4) first, then the results are used to solve Eq. (5) to include the viscous effects. According to Ref. 19, the flux-coordinate splitting technique is capable of giving infinite resolution to the contact discontinuity. Since central difference is used to discretize the viscous terms in Eq. (5), a possible smearing of the contact discontinuity could result. This will depend on the relative magnitudes of the viscous stresses and heat fluxes and their spatial derivatives. For air, μ and k at NTP are about 1.7×10^{-5} kg/m · s and 2.8×0^{-2} W/m · K, respectively, and vary with temperature by a factor of 2 over a range of about 500°C. Furthermore, only $\bar{\mu}$ and $\bar{k}$ are used in the calculations. On the other hand, ρ is of order 1 kg/m^3 in the same temperature range. The present calculations show that the spatial derivatives of the viscous stresses and heat fluxes are very small compared to other terms in Eq. (5). Consequently, the viscous terms do not contribute significantly to the smearing of the contact discontinuity, and the outcome is an indistinguishable difference between the FCS-E and FCS-NS resolved contact discontinuity.

The ENO results[13] show that the contact discontinuity is smeared over several grid cells (Fig. 2), in spite of the use of higher-order accurate numerical schemes. Resolution is improved to 2-3 grid cells when the low initial pressure ratio case is calculated (Fig. 6). This means that the accuracy of the ENO scheme is problem dependent whereas the present technique is not. On the other hand, the ENO/ACM and ENO/subcell results give a 2-3 grid cell resolution of the contact discontinuity for both cases and are in very good agreement with the present calculations.

The shock is smeared over 6-7 grid cells (Figs. 2-6) as a result of viscous effects and numerical truncation error. Essentially, there is little difference between the FCS-E and FCS-NS solutions. The expansion fan is calculated correctly with the exception of some rounding at the knee (trailing edge of the fan). Viscous effects also contribute to the rounding. Consequently, the Navier-Stokes results show a slightly worse comparison with the exact solutions. The Euler solutions obtained from the various ENO schemes give a resolution of 4-5 grid cells for the shock and a rounding at the trailing edge of the expansion fan. In view of this, the present technique compares favorably with other numerical schemes in the calculation of the rest of the flowfield. Therefore, it can be said that the present technique represents an improvement in accuracy over existing techniques because of its ability to calculate contact discontinuities wtih infinite resolution. Another numerical technique[17] that is capable of calculating shocks and contact discontinuities with infinite resolution is based on the random choice method.[14,15] However, that technique can only give the averaged positions of the shocks and contact discontinuities. Besides, its extension to two-dimensional, viscous internal flow is not straightforward.

Mixing of Two Supersonic Streams

The idealized problem involves the mixing of two streams with different initial pressures, densities and velocities sepa-

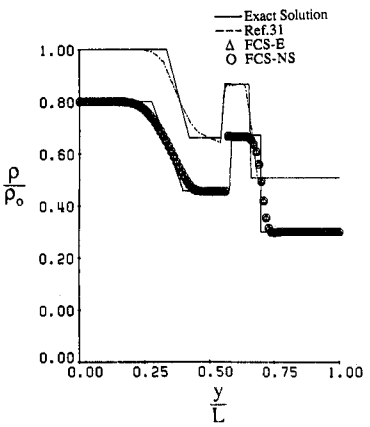

Fig. 7 Density profile across the mixing layer a $x/L = 0.5$.

rated by a splitter plate. When steady state has been reached, a shock is formed on the low pressure side downstream of the splitter plate, while an expansion fan propagates into the high pressure side. A contact discontinuity is formed in the flow between the shock and the expansion fan. The calculations are carried out for the following initial conditions: pressure and density ratios of 4 and 2, respectively, a Mach number of $M_x = 4$ on the low-pressure side and a $M_x = 2.4$ on the high pressure side. Perfect gas with $\gamma = 1.4$ is assumed. These initial conditions are the same as those reported in Refs. 30 and 31. In Ref. 31, a Lagrangian method is used to solve the equations. Consequently, the results give a much sharper resolution of the contact discontinuity compared to those given in Ref. 30. Therefore, besides comparing with the exact solution,[29] the present calculations are also compared with the Lagrangian results given in Ref. 31. Again, two sets of calculations are made, one with FCS-E and another with FCS-NS. This way, viscous effects on the smearing of the contact discontinuity can be assessed.

The unsteady equations are solved and steady state solution is achieved when the solutions of two consecutive time steps are essentially equal. If Δt is the time step such that $t = n\Delta t$ and Δx and Δy define the grid sizes such that $x = j\Delta x$ and $y = k\Delta y$, then Δt is chosen to be

$$\Delta t = (\text{CFL}) \min [(\Delta t)_L, (\Delta t)_E] \tag{19}$$

where $(\Delta t)_L$ and $(\Delta t)_E$ are given by Ref. 19 as

$$(\Delta t)_E = \left[(\sqrt{W_x^2 + W_y^2} + a)_{\max} (\Delta x^{-2} + \Delta y^{-2})^{1/2}\right]^{-1} \tag{20a}$$

$$(\Delta t)_L = 1/\{(a\rho)\min[\Delta\xi^{-1}, \Delta\eta^{-1}]\} \tag{20b}$$

and $\Delta\xi$ and $\Delta\eta$ are the transformed Δx and Δy. In the following calculation, $\Delta x (= \Delta\xi) = \Delta y\ (= \Delta\eta) = 0.01L$ are specified, where L is an arbitrary length scale. The calculation domain is chosen to be bounded by $0 < x/L \leq 1$ and $0 \leq y/L \leq 1$. A CFL = 0.1 is found to give stable solutions, therefore this CFL value is used for all calculations. In principle, nine-point interpolation and extrapolation formulas are required if the fluid properties on either side of the contact discontinuity are to be determined to second-order accuracy. However, according to the procedure described earlier, only three-point interpolation and extrapolation formulas are used. This choice affects numerical accuracy and convergence rate but greatly simplifies numerical complexities. Since the contact discontinuity is calculated with infinite resolution, this sacrifice in numerical accuracy is not important to the overall results. On the other hand, a penalty has to be paid on the convergence rate. This is why a CFL = 0.1 is necessary for stable solution of the governing equations.

When the coordinate splitting technique is suppressed, the flux-vector splitting technique is capable of capturing the shock, the contact discontinuity, and the expansion fan. However, in this case the shock is captured within 4–5 grid cells and the contact discontinuity is captured within 8–9 grid cells. The location of the centerpoint of the spread of the contact discontinuity is taken to be its approximate location and the coordinate splitting technique is applied to sharpen the resolution of the discontinuity calculation. This way, the difficulty of capturing the contact discontinuity in the flux-coordinate splitting calculation can be avoided and the location of the contact discontinuity is captured to within one grid cell.[19] Therefore, the following calculations are first carried out with the coordinate splitting technique suppressed and then again with the use of the flux-coordinate splitting technique. These last results are shown in Figs. 7–9. It should be pointed out that 820 iteration are required for the FCS-E solution, whereas 30 more iterations are necessary for the FCS-NS calculations. Therefore, most of the CPU time is spent on determining the base solution. The sharpening of the contact discontinuity only takes up a very small fraction of the total CPU time.

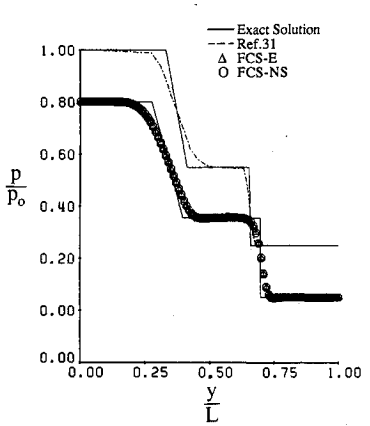

Fig. 8 Pressure profile across the mixing layer at $x/L = 0.5$.

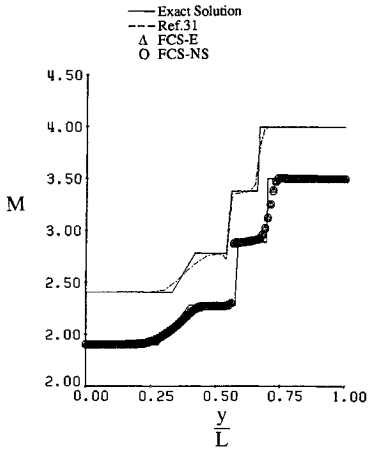

Fig. 9 Total Mach number (M) profile across the mixing layer at $x/L = 0.5$.

The present solutions are compared with the exact solution[29] and with those obtained from a Lagrangian technique.[31] These results are plotted separately (displaced by one division in Figs 7–9) from the present calculations to avoid clutter. For ease of comparison, the exact solutions are also shown in each plot drawn in Figs. 7–9.

Up to now, the best resolution of the contact discontinuity in this steady, two-dimensional flow is given by the method of Loh and Hui.[31] It is obtained by solving the Euler equations. Even then, the resolution is no better than 3 grid cells (Fig. 7). In Fig. 7, there is a mismatch in the x/L locations for the present results and those of Ref. 31. The reason is that the Lagrangian results are not obtained along the same y coordinate. The extension of their method to handle Navier-Stokes equations is not immediately obvious and has not been attempted. The present technique gives an infinite resolution for the contact discontinuity, and the methodology used to treat the Navier-Stokes equations could be extended to three-dimensional flows. This can be accomplished in the following manner. The method of fractional steps is used to split the governing equations into a set of three-dimensional Euler equations and a diffusion-type equation. The Euler equations could be solved by a generalized flux-vector splitting technique[9,32] to provide a three-dimensional base solution for the application of the FCS-NS technique. Therefore, the approximate location of the contact discontinuity surface is again known. Since the flux-coordinate splitting technique[19] is formally based on the method of fractional steps, it could be logically extended to handle three-dimensional Euler equations. A straightforward generalization of Richtmyer and Morton's transformation[23] again allows the split equations to be transformed to Lagrangian equations with no explicit density dependence on the spatial derivate. Therefore, the resultant equations can be solved using the numerical procedure of Ref. 19.

The calculation of the shock and expansion fan using the present technique compares favorably with that of Ref. 31 and with the exact solution (Figs. 8 and 9). As expected, the numerical calculations show a rounding at the leading and trailing edges of the expansion fan. Again, viscous effects do not contribute to the smearing of the contact discontinuity (Fig. 7). These results demonstrate that with proper treatment of the equations before discretizing, numerical smearing of the contact discontinuity could be eliminated even when a second-order accurate finite-difference scheme is used. In addition, the technique could be logically extended to three-dimensional flows. These attributes argue well for the development of the flux-coordinate splitting technique as an alternative for the calculation of three-dimensional, viscous compressible flows.

V. Conclusions

A flux-coordinate splitting technique has been previously formulated to treat unsteady, two-dimensional Euler equations.[19] The technique is based on flux-vector splitting to capture shocks and on the method of fractional steps plus a generalized Richtmyer and Morton transformation to sharpen contact discontinuities in the flow. This combination gives an accurate resolution of the shocks and an infinite resolution of the contact discontinuities. The present paper extends this technique to treat unsteady, two-dimensional Navier-Stokes equations. A formal procedure based on the method of fractional steps is used to split the Navier-Stokes equations into a set of Euler equations and a diffusion-type equation. The Euler equations are solved by the flux-coordinate splitting technique, whereas a second-order accurate central difference scheme is used to treat the diffusion-type equation. As expected, for gasdynamic flows, viscous effects do not contribute to the smearing of the contact discontinuity and infinite resolution of the contact discontinuity in a shock tube flow and a two-dimensional supersonic mixing flow is again obtained. In every respect, the results are comparable or better than other numerical solutions, including those given by ENO/ACM,[13] ENO/subcell,[13] and a Lagrangian method.[31] The present technique has been applied to calculate practical flows[18] and can be extended to solve unsteady, three-dimensional Navier-Stokes equations because the method of fractional steps can be logically formulated to handle m-dimensional flows. In view of this, it is an attractive alternative to the more established numerical techniques.

Acknowledgments

The authors acknowledge support from the Research Incentive Award of the Arizona State University, the Garrett Thermal Science Award, and David Taylor Research Center, Annapolis, MD, under Contract N00167-86-k-0075.

References

[1]Steger, J. L., and Warming, R. F., "Flux Vector Splitting of the Inviscid Gasdynamic Equations with Applications to Finite-Difference Methods," *Journal of Computational Physics*, Vol. 40, 1981, pp. 273–293.

[2]Van Leer, B., "Flux-Vector Splitting of the Euler Equations," *Lecture Notes in Physics*, Vol. 170, edited by H. Avaki, J. Ehlers, K. Hepp, R. Kippenhahn, H. A. Weidenmuler, and J. Zittarta, Springer-Verlag, Berlin, 1982, pp. 507–512.

[3]Buning, P. G., and Steger, J. L., "Solution of the Two-Dimensional Euler Equations with Generalized Coordinate Transformation Using Flux Vector Splitting," AIAA Paper 82-0971, 1982.

[4]Anderson, W. K., Thomas, J. L., and VanLeer, B., "A Comparison of Finite Volume Flux-Vector Splitting for the Euler Equation," AIAA Paper 85-0122, 1985.

[5]Moretti, G., "The λ-Scheme," *Computers & Fluids*, Vol. 7, 1979, pp. 191–195.

[6]Chakravarthy, S. R., Anderson, D. A., and Salas, M. D., "The Split Coefficient Matrix Method for Hyperbolic Systems of Gasdynamic Equations," AIAA Paper 80-0278, 1980.

[7]Yang, J. Y., Lombard, C. K., and Bershader, D., "Numerical Simulation of Transient Inviscid Shock Tube Flows," *AIAA Journal*, Vol. 25, 1987, pp. 245–251.

[8]Scott, J. N., and Hankey, W. L., Jr., "Navier-Stokes Solution of Unsteady Flow in a Compressor Rotor," *Journal of Turbomachinery*, Vol. 108, 1986, pp. 206–215.

[9]Grossman, B., and Walters, R. W., "Flux-Split Algorithms for the Multi-Dimensional Euler Equations with Real Gases," *Computers & Fluids*, Vol. 17, 1989, pp. 99–112.

[10]Dadone, A., Fortunato, B., and Laaippolis, A., "A Fast Euler Solver for Two- and Three-Dimensional Internal Flows," *Computers & Fluids*, Vol. 17, 1989, pp. 25–37.

[11]Harten, A., "The Artificial Compression Method for Computation of Shocks and Contact Discontinuities. I Single Conservation Laws," *Communication in Pure and Applied Mathematics*, Vol. 30, 1977, pp. 611–638.

[12]Harten, A., Engquist, B., Osher, S. and Chakravarthy, S. R., "Uniformly High-Order Accurate Essentially Non-Oscillatory Schemes, III," *Journal of Computational Physics*, Vol. 71, 1987, pp. 271–303.

[13]Shu, C. W., and Osher, S., "Efficient Implementation of Essentially Non-Oscillatory Shock Capturing Schemes, II," *Journal of Computational Physics*, Vol. 83, 1989, pp. 32–78.

[14]Chorin, A. J., "Random Choice Solution of Hyperbolic Systems," *Journal of Computational Physics*, Vol. 22, 1976, pp. 517–533.

[15]Glimm, J., "Solution in the Large for Non-Linear Hyperbolic Systems of Equations," *Communication in Pure and Applied Mathematics*, Vol. 28, 1965, pp. 697–715.

[16]Sod, G. A., "A Numerical Study of a Converging Cylindrical Shock," *Journal of Fluid Mechanics*, Vol. 83, 1977, pp. 785–794.

[17]Sod, G. A., "A Survey of Several Finite Difference Methods for Systems of Nonlinear Hyperbolic Conservation Laws," *Journal of Computational Physics*, 27, 1978, pp. 1–31.

[18]Zhang, H. S., and So, R. M. C., "Calculation of the Material Interface in a Pressure-Wave Supper Charger," *Institute of Mechanical Engineers, Proceedings Part A, Journal of Power and Energy*, Vol. 204, 1990, pp. 151–161.

[19]Zhang, H. S., and So, R. M. C., "A Flux-Coordinate Splitting Technique for Flows with Shocks and Contact Discontinuities," *Computers and Fluids* (to be published).

[20]Peaceman, D. W., and Rachford, H. H., Jr., "The Numerical Solution of Parabolic and Elliptic Differential Equations," *SIAM Journal*, Vol. 3, 1955, pp. 28–41.

[21]Yanenko, N. N., "The Method of Fractional Steps for Numerical Solution of the Problems of Mechanics of Continous Media," *Fluid Dynamics Transaction*, Vol. 4, Inst. of Fundamental Technical Research, Polish Academy of Science, Warsaw, Poland, pp. 135–147.

[22]MacCormack, R. W., "Numerical Solution of the Interaction of a Shock Wave with a Laminar Boundary Layer," *Lecture Notes in Physics*, Vol. 8, pp. 151–163.

[23]Richtmyer, R. D., and Morton, K. W., *Difference Methods for Initial-Value Problems*, 2nd Edition, Interscience, New York, 1967, p. 295.

[24]Reklis, R. P., and Thomas, P. D., "Shock-Capturing Algorithm for the Navier-Stokes Equation," *AIAA Journal*, Vol. 19, 1982, pp. 1212–1218.

[25]MacCormack, R. W., "Current Status of Numerical Solution of the Navier-Stokes Equations," AIAA Paper 85-0032, 1985.

[26]Abaranel, S., Duth, P., and Gottlieb, D., "Splitting Methods for Low Mach Number Euler and Navier-Stokes Equations," *Computers & Fluids*, Vol. 17, 1989, pp. 1–12.

[27]MacCormack, R. W., "The Effect of Viscosity in Hypervelocity Impact Cratering," AIAA Paper 69-0354, 1969.

[28]Liepmann, H. W., and Roshko, A., *Elements of Gasdynamics*, Wiley, New York, 1957, p. 79.

[29]Owczarck, J. A., *Fundamentals of Gas Dynamics*, International Textbook Co., Scranton, PA, 1964, p. 435.

[30]Glaz, H. M., and Wardlaw, A. B., "A Higher-Order Godunov Scheme for Steady Supersonic Gas Dynamics," *Journal of Computational Physics*, Vol. 58, 1985, pp. 157–187.

[31]Loh, C. Y., and Hui, W. H., "A New Lagrangian Method for Steady Supersonic Flow Computation, Part I: Godunov Scheme," *Journal of Computational Physics*, Vol. 89, 1990, pp. 207–240.

[32]Anderson, W. K., Thomas, J. L., and Rumsey, C. L., "Extension and Applications of Flux Vector Splitting to Unsteady Calculations of Dynamic Meshes," AIAA Paper 87-1152, 1987.